

High resolution crystal structure of ferricytochrome c' from *Rhodobacter sphaeroides*

Laura M.-Ramirez,^(1,2) Herbert L. Axelrod,^(1,3) Steven R. Herron,⁽¹⁾ Bernhard Rupp,⁽⁴⁾ James P. Allen,⁽⁵⁾ and Katherine A. Kantardjiev^{(1)*}

Received August 6, 2002

Cytochrome c' isolated from *Rhodobacter sphaeroides* strain R26 (RSCP) crystallizes as a dimer of two identical 14-kDa subunits, in trigonal space group $P3_1$, with cell parameters $a, b = 48.10 \text{ \AA}$, $c = 115.80 \text{ \AA}$. The crystal structure of RSCP has been solved by molecular replacement using cytochrome c' from *Rhodobacter capsulatus* (PDB ID: 1CPQ) as a search model. To ensure effective phase bias removal, the RSCP model was iteratively built into maps generated by a modified *wARP* procedure, *Shake&wARP*. The 1.8 \AA model (PDB ID: 1GQA) has been refined to an $R = 0.204$ and $\text{free}R = 0.254$. Each subunit consists of four antiparallel α -helices, with the pentacoordinate heme covalently bound to a C–X–Y–C–H motif near the C-terminus. F14, located on helix A, blocks direct access to what would be the sixth “distal” ligand binding site of the heme. The dimer subunits form a flattened “X” shape, intermediate between the Type 1 and Type 2 cytochromes c' . The presence of the aromatic F14 and a deep channel between helices B and C places RSCP into Group 1 cytochromes c' . Clear electron density has revealed that the amino acid sequences for the cytochrome c' from strains R26 and 2.4.1 are identical.

KEY WORDS: Cytochrome c' ; heme protein; four helix bundle; *Rhodobacter sphaeroides*.

Introduction

Cytochromes c' are paramagnetic heme proteins found in the periplasmic space of phototrophic and denitrifying bacteria, and these pro-

teins are the largest and most widespread class (IIa) of bacterial c-type cytochromes.¹ Although cytochromes c' are alleged to function as electron carriers with a pH-dependent reduction potential that ranges from -10 to $+150 \text{ mV}$,^{2,3} their exact physiological role remains unclear. Several recent studies suggest that cytochromes c' may help to alleviate nitrosative stress in bacteria.^{4,5} Cytochromes c' have been shown to have highly conserved physicochemical and structural properties over a wide range of bacterial species, but extensive sequence homology is generally restricted to the carboxyl terminal region incorporating the heme binding sequence C–X–Y–C–H similar to that of low spin cytochromes c .⁶ However, the cytochromes c' exhibit little sequence homology

⁽¹⁾ Department of Chemistry and Biochemistry and W.M. Keck Foundation Center for Molecular Structure, California State University, Fullerton, California 92834.

⁽²⁾ Present address: John Bosco Technical Institute, Rosemead, California.

⁽³⁾ Present address: Department of Physics, University of California San Diego, La Jolla, California.

⁽⁴⁾ Macromolecular Crystallography and Structural Genomics, Lawrence Livermore National Laboratory, Livermore, California.

⁽⁵⁾ Department of Chemistry and Biochemistry, Arizona State University, Tempe, Arizona.

* To whom correspondence should be addressed. E-mail: kkantardjiev@fullerton.edu

to the soluble class I cytochromes *c* from mitochondria.

Cytochromes *c'* occur primarily as 28-kD homodimers, although those from *Rhodobacter sphaeroides* and *Rhodobacter capsulatus* have been shown to exist as an equilibrium mixture of monomers and dimers in solution, and cytochrome *c'* from *Rhodopseudomonas palustris* is completely monomeric.^{3,7} Each monomer chain folds into an elongated right-handed four α -helix bundle⁸ incorporating the covalently bound heme. The heme iron is pentacoordinate and, as observed in other high spin cytochromes such as globins and cytochrome *c* peroxidase, the sixth ligand position is vacant.⁹ The heme iron is high spin ($S = 5/2$) and paramagnetic in both the Fe^{2+} (reduced) and Fe^{3+} (oxidized) states, although the ferric ions have been proposed to exist as mixed spin states ($S = 5/2$ and $S = 3/2$) at neutral pH.¹⁰ The heme pocket in cytochromes *c'* is small and largely composed of hydrophobic side groups.^{9,11–16} Monomers typically bind ligands such as CO and NO axially to the heme in both the oxidized and reduced forms.^{17,18} Recent crystallographic studies on cytochrome *c'* from *Alcaligenes xyloxidans* have revealed that exogenous ligands such as NO exhibit a novel proximal coordination geometry, with NO residing at the previously occupied axial histidine binding site.¹⁸ Binding of CO has been shown to bring about conformational changes that result in dissociation of dimer to monomer.¹⁷ Thus, cytochromes *c'* provide models for the electronic environment of heme proteins, as well as for cooperative interactions in proteins.

Here we report the structure of RSCP at 1.8-Å resolution, determined by single crystal X-ray diffraction. To date the crystal structures of cytochromes *c'* from *Rhodopseudomonas palustris* (RPCP),⁹ *Rhodospirillum molischanum* (RMCP),^{11,12} *Chromatium vinosum* (CVCP),¹³ *Rhodospirillum rubrum* (RRCP),¹⁴ *Alcaligenes xylooxidans* NCIB 1105 (AXCP),¹⁵ *Alcaligenes dentrificans* (ADCP),¹⁶ *Rhodocyclus gelatinosus* (RGCP),¹⁶ and *Rhodobacter capsulatus* (RCCP)¹⁹ have been reported. The unique

structural features of RSCP will be described, and the structure will be compared to other cytochromes *c'*.

Experimental

Purification and crystallization

Cytochrome *c'* was prepared from *Rhodobacter sphaeroides* strain R26 using a procedure modified from that reported by Bartsch,^{2,20} and then dialyzed against 50-mM phosphate buffer, pH 4.5. Crystals were grown by the hanging drop vapor diffusion method at room temperature. Crystallization conditions were identified with Hampton Research Crystal ScreenTM, formulation 42. Crystals suitable for X-ray diffraction analysis were observed within 1 week in hanging drops containing 10 μL of protein solution (20 mg/mL in 50-mM sodium phosphate buffer, pH 4.5) and 10 μL precipitant solution (20% (w/v) polyethylene glycol (PEG) 8000 and 50-mM sodium phosphate, pH 4.5) equilibrated against 1-mL reservoirs of precipitant solution.

X-ray analysis

Diffraction data (Cu $K\alpha$ radiation, graphite monochromator) were collected nominally to 1.5 Å at room temperature from a crystal mounted in a 0.7-mm quartz capillary on a Rigaku R-Axis IIC imaging plate detector system (Table 1). Diffraction data from each 1° of oscillation were recorded for 30 min. Data were integrated and scaled with the R-Axis IIC data processing software suite.²⁵ Crystals belong to space group $P3_1$, no. 144, with cell parameters $a, b = 48.10 \text{ \AA}, c = 115.80 \text{ \AA}$. The two molecules comprising the dimer are related by a twofold non-crystallographic symmetry (NCS) axis very nearly perpendicular to the c axis, close but not identical to the crystallographic twofold axes in $P3_121$.

Starting phases were obtained by molecular replacement using the structure of RCCP (PDB

Table 1. Data Collection and Refinement Statistics

Data Collection	
Space group	<i>P</i> 3 ₁
Wavelength (Å)	1.54178
Temperature (K)	293
<i>a</i> , <i>b</i> (Å)	48.10
<i>c</i> (Å)	115.80
Resolution (Å)	31.00–1.80
Observed reflections ^a	67416 (5617)
Unique reflections ^a	24077 (2553)
% Completeness	87 (57)
Rsym ^a	0.10 (0.16)
$\langle I/\sigma(I) \rangle$ ^a	8.1 (4.6)
<i>V</i> _m (Matthews coefficient)	2.9
% Solvent	57
Refinement	
Free <i>R</i> value ^a , random, 10%	0.254 (0.351)
<i>R</i> value ^a	0.204 (0.271)
No. of protein atoms	1913
No. of water molecules	291
No. of heterogen atoms	86
rmsd bond length (Å) ^b	0.019
rmsd bond angle (°) ^b	1.745
Overall coordinate error (Å) ^c	0.162
RSCC (<i>Shake&wARP</i>) ^d	0.93
RSCC (<i>Refmac5</i>) ^e	0.94

Note: Additional details about chemical restraints and refinement parameters are available in the Protein Data Bank file 1GQA.

^aValues in parenthesis for the highest resolution bin (1.85–1.80 Å).

^bDeviations from restraint targets.²¹

^cEstimated standard uncertainty, Diffraction Precision Index (DPI) based on free*R*²².

^dReal space correlation coefficient, averaged and weighted *Shake&wARP* map against *F*_c map.

^eReal space correlation coefficient, maximum likelihood *mF*_o – *DF*_c map, reported by *Refmac5*.^{23,24}

ID: 1CPQ; 41% sequence identity) as a search model. *Epmr*²⁶ was used in default automated partial structure mode searching for two molecules in the asymmetric unit (12–4 Å data). The search for the first molecule converged at a correlation coefficient (CC) of 0.27. Using partial structure factors based on the position of molecule one, the search for the second molecule in the asymmetric unit reached convergence within five iterations (CC = 0.44, *R* = 0.51). Rigid body refinement of the two individual molecules against 2.8 Å data slightly improved CC to 0.47 (*R* = 0.50).

To ensure effective phase bias removal, the RSCP model was iteratively built into

maps generated by a modified *wARP* procedure, *Shake&wARP*.²⁷ Six different starting models were created by randomly deleting 10% of all atoms and randomly perturbing the atomic coordinates by 0–0.5 Å (rmsd 0.25 Å). Dummy atoms were automatically built into each model using *ARP*²⁸ followed by unrestrained maximum likelihood refinement with *Refmac5*.^{23,24} After 30 cycles, the resulting six individual maps were averaged, and structure factor weights (*w*) and weighted phases were calculated as described in Perrakis *et al.*²⁹ The model was iteratively rebuilt into the resulting weighted electron density maps using the program *Xfit* in the *XtalView* package.³⁰ Residues or regions with significantly different conformations in the two molecules were excluded from NCS restraints during refinement. After repeated cycles of water building using *ARP* and real space refinement using *Xfit*, followed by restrained *Refmac5* maximum likelihood refinement, the final structure (PDB ID: 1GQA) refined to *R* = 0.204 and free*R* = 0.254. For each of the intermediate models, real space correlation coefficient plots (Fig. 1) were calculated from *Shake&wARP* maps using *Overlapmap* in the CCP4 suite and in-house programs.²⁷

Results and discussion

Overall structure

Electron density was extremely clear and continuous for both molecules in the asymmetric unit, and side chain conformations, including alternate conformations, could be resolved for all 130 residues except R130 at the C-terminus. The final model has excellent stereochemistry (Fig. 2) and fits well to the electron density, with an overall real space correlation coefficient of 0.94 (Fig. 1(B)). During model building, an inconsistency was noted between the reported sequence for RSCP¹ and the exceptionally clear electron density in helix D. The sequence 116–119 in strain R26 is GGTC rather than GTGC

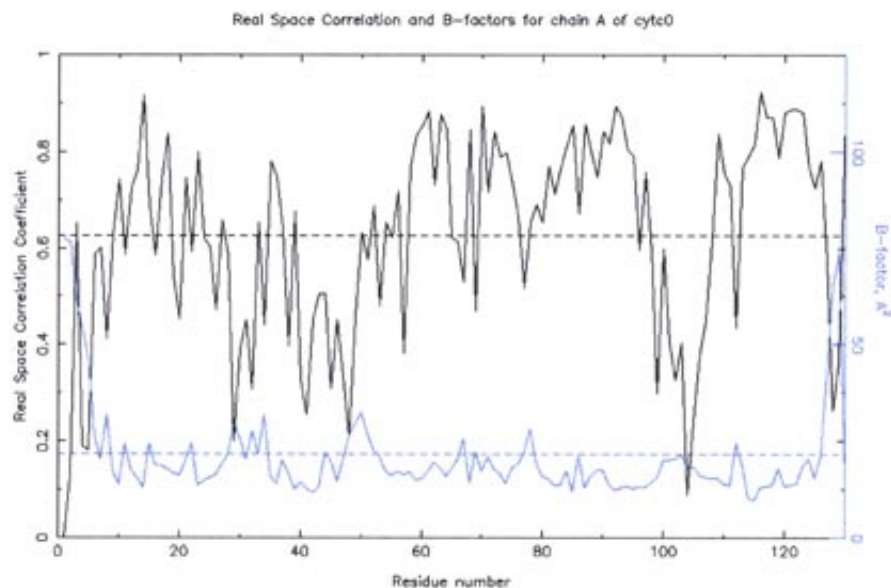
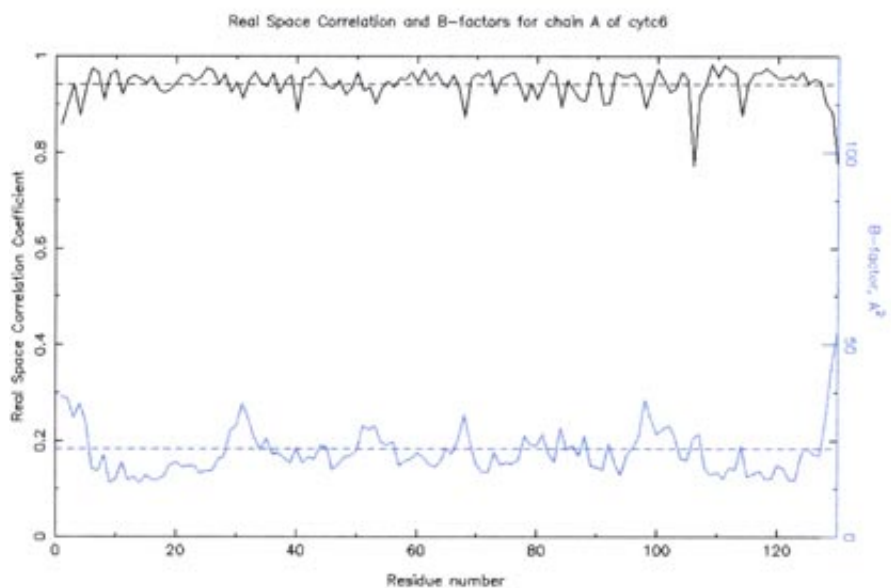
**A****B**

Fig. 1. (A) Improvement of model quality during rebuilding of the RSCP model. Poor real space correlation (upper graph) of the fit between each residue of the initial model and the *Shake&wARP* bias-minimized electron density map directly after molecular replacement. (B) Real space correlation of the fit (upper graph) between the final model and final *Shake&wARP* bias-minimized electron density map. Lower graphs in (A) and (B) show B factors.

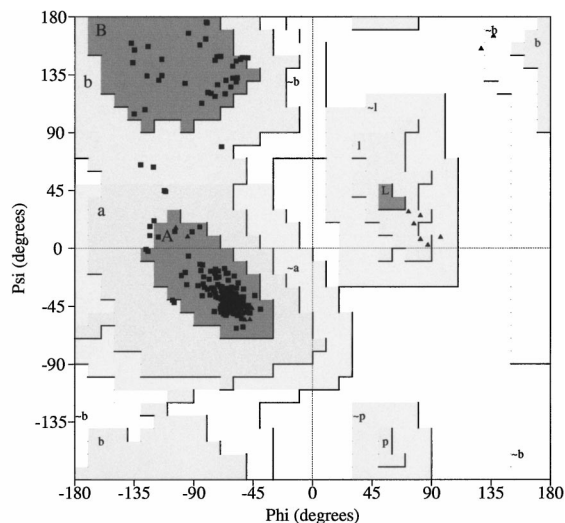


Fig. 2. Ramachandran plot showing stereochemical quality of the RSCP structure. Triangles represent glycines, squares all other residues. No residues are found in disallowed regions, and 95.5% of residues have phi and psi backbone torsion angles within the most favored regions, as defined by PROCHECK.³¹

as reported for strain 2.4.1 in SWISS PROT (Fig. 3). Comparison with the more recently determined genomic sequence from strain 2.4.1^{32–34} confirms that this error is probably typographical, and that the sequences of cytochrome *c'* from *Rhodobacter sphaeroides* strains R26 and 2.4.1 are identical.

As in other cytochromes *c'*, the RSCP monomer consists of four antiparallel α -helices (A–D) with the heme group covalently incorporated in the concavity of the helical bundle (Fig. 4). Helix A in RSCP is noticeably bent at P23, a feature also seen in RPCP. Helix C in RSCP is bent at P99, a residue unique among the cytochromes *c'* at this position. Three additional prolines are found in the loop regions, P33 in the AB loop, and P54 and P60 both in the BC “flexible” loop. The four α -helices bundle topology of RSCP is intermediate between the more conical arrangement of helices seen in CVCP, which also has prolines in helix and loop regions, and the more parallel arrangement seen in RCCP, where prolines are found only in the flexible loop region.

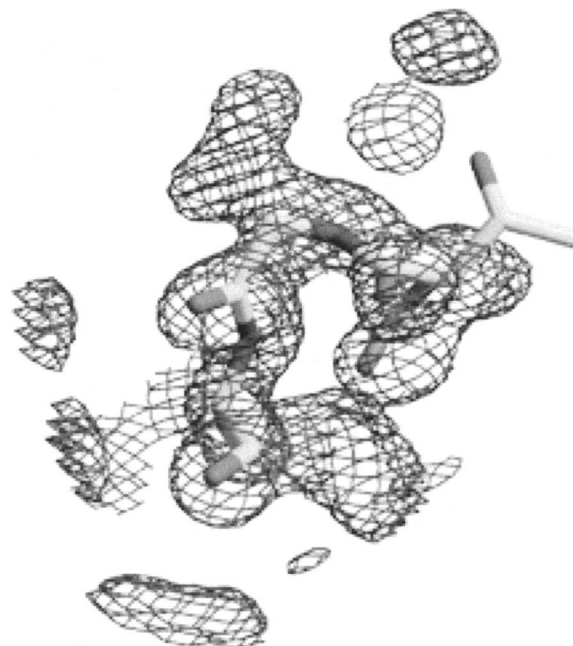


Fig. 3. Overlay of residues 116–119 of reported sequence in SWISS-PROT³ for RSCP strain 2.4.1 with electron density for strain R26. Sequence error in RSCP strain 2.4.1 is identified by clear electron density for a threonine side chain at position 118. The error probably results from a typographic transposition of the sequence, amino acids 116–119 GTGC³ should be GGTC, as confirmed by comparison with more recently determined genomic sequence for strain 2.4.1.^{32–34} Sequences of cytochrome *c'* from strains R26 and 2.4.1 are identical. Combined *Shake&wARP* map. 1.8 Å data, 1 σ electron density level in gray, rendered with *XtalView*.³⁰

Dimer topology and interface

Cytochromes *c'* are distinguished by their dimer topology, which has been attributed to the charge disposition at the A/B dimer interface.⁹ In the classic “X” shaped Type 1 dimer,⁹ such as CVCP, the subunits cross each other at roughly right angles to each other when viewed perpendicularly to the noncrystallographic dyad, with helix crossing angles³⁵ $\Omega(A/A') = -125^\circ$, $\Omega(B/B') = -149^\circ$, and the charged residues are disposed at the loop ends. The central region of the dimer interface consists of a hydrophobic “patch” in which both A/A' and B/B' helices interact. An aromatic or aliphatic hydrophobic residue on helix A blocks

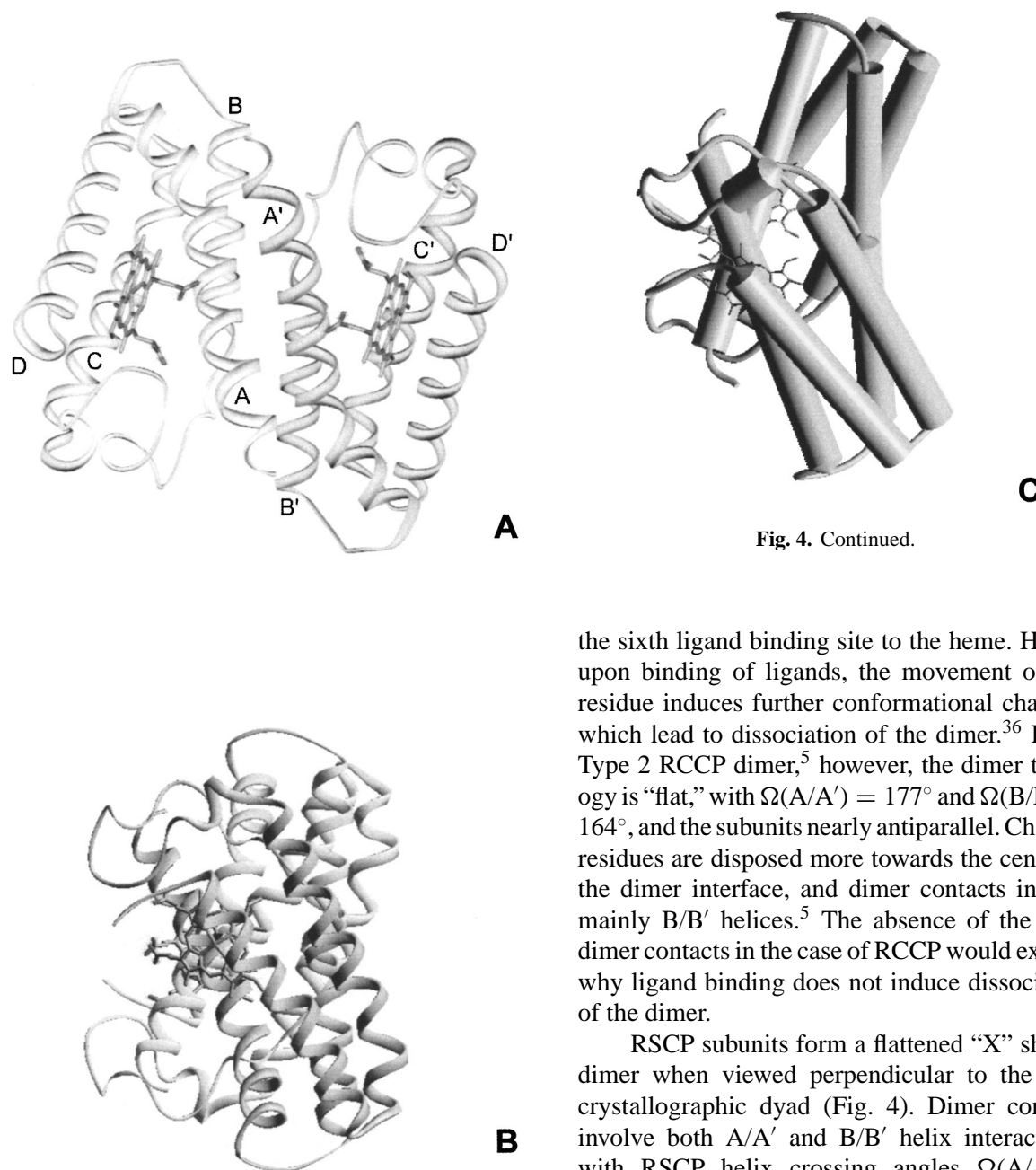


Fig. 4. *Rhodobacter sphaeroides* cytochrome *c'* dimer. (A) Dimer is viewed along the twofold NCS axis. Helices are labeled A–D and A'–D' on each monomer. (B) Dimer is viewed perpendicular to the twofold NCS axis, located horizontally. (C) Same view as in (B), rendered schematically with helices shown as rods for clarity. Images rendered with WebLabViewerLite©v4.2.

the sixth ligand binding site to the heme. Hence, upon binding of ligands, the movement of this residue induces further conformational changes, which lead to dissociation of the dimer.³⁶ In the Type 2 RCCP dimer,⁵ however, the dimer topology is “flat,” with $\Omega(A/A') = 177^\circ$ and $\Omega(B/B') = 164^\circ$, and the subunits nearly antiparallel. Charged residues are disposed more towards the center of the dimer interface, and dimer contacts involve mainly B/B' helices.⁵ The absence of the A/A' dimer contacts in the case of RCCP would explain why ligand binding does not induce dissociation of the dimer.

RSCP subunits form a flattened “X” shaped dimer when viewed perpendicular to the non-crystallographic dyad (Fig. 4). Dimer contacts involve both A/A' and B/B' helix interactions, with RSCP helix crossing angles $\Omega(A/A') = -143^\circ$, $\Omega(B/B') = -172^\circ$. In helix A (residues 2–29), there are 12 hydrophobic interactions and three hydrogen bond interactions with helix A' in the sequence range 5–19, and in helix B (residues 35–52) there are 10 hydrophobic interactions and four hydrogen bond interactions with helix B' in the sequence range 42–52, as indicated by the program, CSU.³⁷ Two

additional hydrophobic dimer interactions of the A/B' type involve L16. With the exception of a water molecule involved in hydrogen bonding with Y13, L49, and Y52, there are no water molecules at the interface that mediate dimer contacts. Because dimer contacts involve the A helices, dissociation upon ligand binding is likely to be similar to that observed in CVCP, where movement of F14 at the vacant position of the heme leads to conformational changes in helix A and disruption of the dimer interface structure.

The dimer topology of RSCP is intermediate between that in Types 1 and 2 cytochromes *c'*, consistent with the charge disposition across the A/B interface (Fig. 5). The hydrophobic contact region between the two RSCP subunits is offset from the center of the interface towards the N-terminal edge of each subunit, and charged residues extend into the interface from the A–B loop end, although not as extensively as in RCCP. The contact surface area in RSCP is comparable to that for

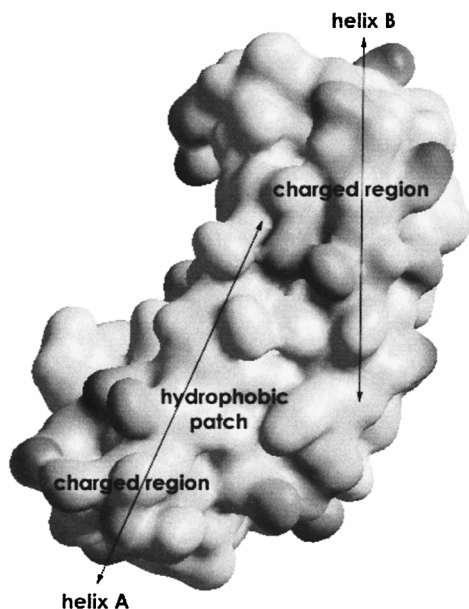


Fig. 5. Charge disposition for RSCP at the dimer interface. Viewed as in Fig. 4(B) but with monomer in front removed from view. Charges are disposed towards the loop ends, and there is a hydrophobic contact region in the lower half of the dimer interface towards the N-terminal edge.

Type 1 cytochromes *c'* such as CCVP and RMCP (approximately 800 \AA^2), and greater than that for RCCP (500 \AA^2). However, the RSCP dimer interface has about 15% more polar residues than CVCP. The interacting surfaces in both RSCP and RCCP exhibit less complementarity and greater planarity than in either CVCP or RMCP.³⁸ Thus, the interface characteristics in RSCP result in a dimer topology that, while still “X” shaped, is flatter in appearance (more antiparallel), intermediate between the two Types. As in the case of RCCP, the disposition of charged groups in RSCP would play a role in establishing an equilibrium mixture of monomer and dimer in solution.^{2,7}

Channel formation between helices B and C

Like other cytochromes *c'* belonging to Group 1,¹⁹ RSCP has both a bulky aromatic side chain near the heme iron sixth ligation position and a deep solvent accessible channel between helices B and C. This channel facilitates the binding of larger ligands, such as ethyl- and *n*-butyl isocyanide, in CVCP³⁶ and RCCP.³⁹ The channel between helices B and C forms partly as a result of amino acid substitutions in these helices. For example, in Group 2 helix B, P55 in RMCP, P53 in RRCP, and W56 in ADCP and AXCP are substituted in Group 1 by G55 in CVCP, A52 in RCCP, and S55 in RSCP. In Group 2 helix C, W86 in RMCP, S83 in RRCP, and Q83 in ADCP and AXCP are substituted in Group 1 by G85 in RCCP, A88 in CVCP, and G87 in RSCP. Group 2 cytochromes *c'* generally have a three–four residue deletion in this region of the amino acid sequence as well. A93 and its equivalent appear to be conserved in Group 1, whereas in Group 2, this residue is substituted by E, N, or L. Because A93 forms an interhelical contact between helices C and D, a larger side chain may shift the position of helix C, closing down the opening of a channel. The aromatic side chain, F14, as well as the edge of the heme and the H123 ligand, are accessible to solvent through the channel in RSCP (Fig. 6). M88 (D, K, or Q in most other cytochromes *c'*), which is located on the molecular surface and near the

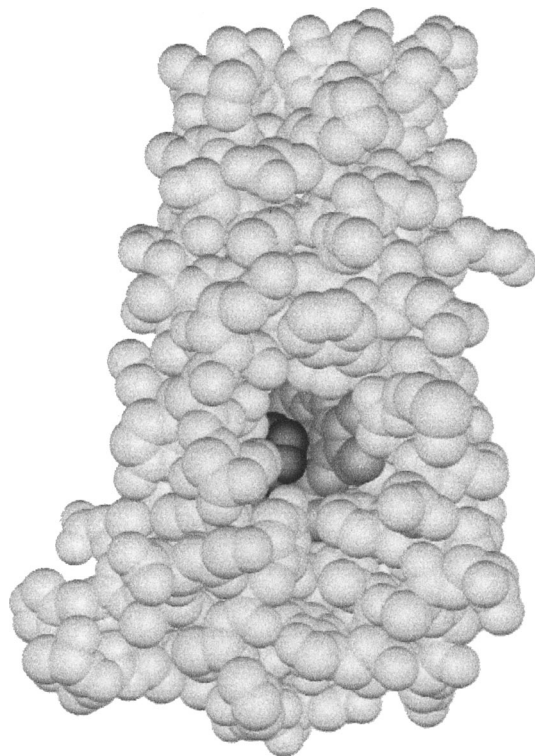


Fig. 6. Solvent accessible channel between helices B and C. A large channel is present between helices B and C, which places RSCP within the Group 1 cytochromes *c'*.¹⁶ In this space filling model, the protein is shown in white CPK spheres, the edge and the distal side of the heme are shown in dark gray spheres, and the aromatic side chain of F14, which blocks the distal ligand binding site, is shown in black spheres. Image rendered with WebLabViewerLite©v4.2.

channel entrance, may influence heme ligation by hindering access to the channel in solution.¹⁹

Heme environment

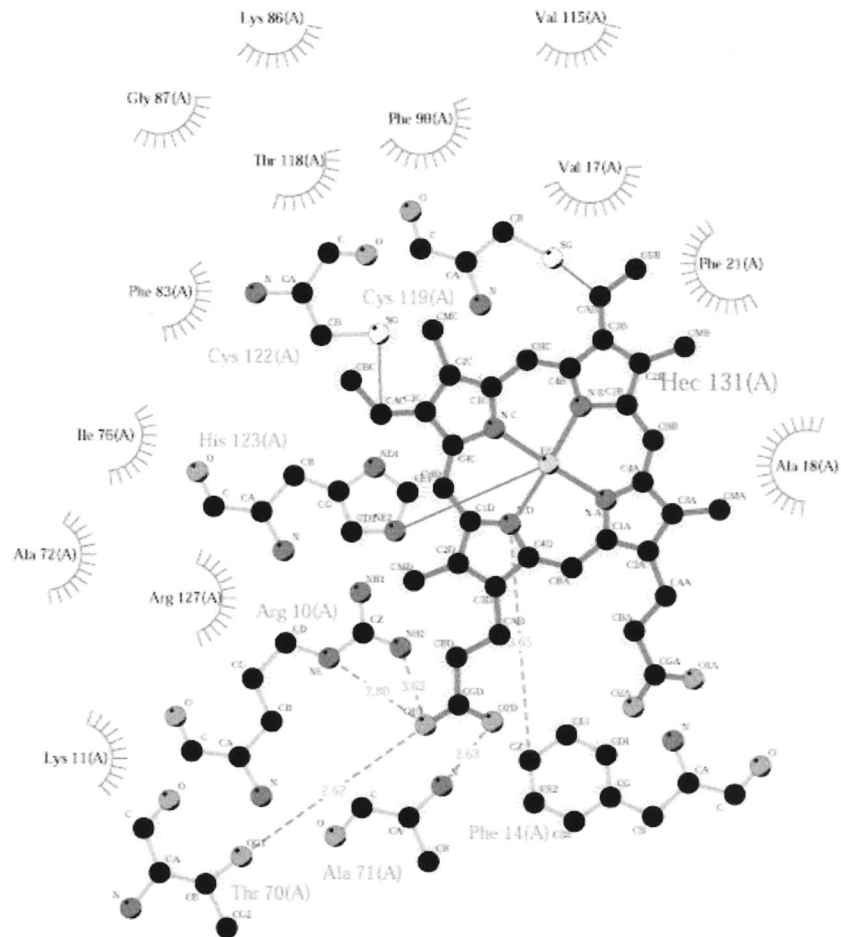
As is typical of *c'*-type cytochromes, the heme in RSCP is covalently bound to the sequence C—X—Y—C—H through thioether linkages between the heme vinyl groups and two cysteine residues on helix D, C119 and C122, near the C-terminus (Fig. 7). The heme iron is pentacoordinate with four pyrrole nitrogen atoms equatorial, NE2 of the H123 imidazole group in an axial position, and F14 from helix A blocking what would

be the sixth “distal” coordination site. As expected for pentacoordinate hemes, the porphyrin ring is puckered towards the histidine ligand, with a Fe—H123 bond length of 2.01 Å. The Fe—Fe distance within the dimer is 24.40 Å.

The heme pocket is primarily hydrophobic, due to van der Waals contacts between the heme and aromatic or aliphatic portions of neighboring residue side chains. Residues constituting the immediate heme contact environment include R10, K11, F14, S15, V17, A18, F21, L46, Y58, T70, A71, A72, I76, F83, K86, G87, F90, V115, T118, C119, C122, H123, R127, and F126 more peripherally through a stabilizing interaction with F83. The inner heme propionate, via O1D, is hydrogen bonded to NE of R10, OH of T70, and the backbone N of A71. It has been suggested that R10, which is conserved in all known cytochrome *c'* structures, is important to incorporation of the heme, the stability of the protein, and possibly the binding of ligands.¹⁹ Except for a single water hydrogen bonded to O2A of the outer propionate of each heme of the dimer, there are no water molecules in the heme pocket or associated with either heme.

Factors that may control heme iron reduction potential

Thirty years ago, Kassner proposed that a more hydrophobic environment in the heme pocket would favor the reduced form of the heme thereby raising the reduction potential,⁴¹ and a theoretical model was proposed for the effects of local nonpolar heme environments on the reduction potentials in cytochromes.⁴² More recent work by various groups on designed six-coordinate heme proteins is building a consensus of factors that modulate the reduction potential of hemes.^{43–47} These factors, whose ΔE_m ranges from 30–210 mV, include (a) local dielectric effects arising from the solvent accessibility of the hemes; (b) the hydrophobicity of the heme pocket; (c) interactions of the heme and heme ligands with surrounding residues. Heme reduction



Key

- | | | | |
|--|------------------------------|--|---|
| | Ligand bond | | His 53 Non-ligand residues involved in hydrophobic contact(s) |
| | Non-ligand bond | | Corresponding atoms involved in hydrophobic contact(s) |
| | Hydrogen bond and its length | | |

Fig. 7. Heme pocket of RSCP. Schematic diagram of protein–heme interactions mediated by hydrogen bonds and by hydrophobic contacts. The heme in RSCP, shown at the center of the figure, is covalently bound to the sequence C–K–Y–C–H through thioether linkages to C119 and C122 near the C-terminus. F14 in helix A, visible below the heme, blocks direct access to what would be the sixth “distal” ligand site. NE2 of the H123 imidazole group binds iron in the axial position. R10, shown at the lower left, is hydrogen bonded via NE to OD2 of the heme propionate. Additional residues that constitute the heme environment are indicated. Image created with LIGPLOT.⁴⁰

potentials of single heme bound states have been found to correlate with apoprotein conformational specificity, demonstrating that hydrophobic packing modulates heme redox activity.⁴⁴ Cytochromes *c'* share a similar four helix bundle structural motif and pentacoordinate heme iron ligation, they exhibit a >100 mV range in reduction potential,^{2,3} and those for which crystal structures have been determined have well described heme microenvironments.^{9,11–16,19} Thus, cytochromes *c'* present an opportunity to consider the role that various aforementioned factors may play in mediating reduction potential.

Solvent accessibility. We have calculated the solvent accessible surface area (ASA)³⁷ for the pentacoordinate hemes in the cytochromes *c'* whose structures have been reported, and we find that there is a weak correlation (0.22) between the ASA and the reported midpoint reduction potential of the heme.^{2,3} One must be cautious, however, to conclude that solvent accessibility is not a determining factor of heme reduction potential. Although cytochromes *c'* maintain a certain degree of structural homology, other factors due to subtle, nonnegligible differences will provide additional energetic contributions.

Hydrophobicity. We next consider the effect that local hydrophobic amino acids may have on the heme reduction potentials. In six-coordinate heme systems, single conservative hydrophobic amino acid modifications local to heme binding sites have been found to modulate heme reduction potentials by as much as 50 mV, although these effects are not strictly additive, because modifications are distant dependent.⁴⁸ When the hydrophathy profiles^{49,50} of the local heme environments and the reported heme reduction potentials for cytochromes *c'* are compared, there is a good correlation (0.7–0.8). Moreover, the contact surface area³⁷ of the heme with local residues correlates well (0.84) with the reported reduction potential, which suggests that for the pentacoordinate hemes, hydrophobic packing is a significant factor in modulating heme redox activity.

Heme–protein interactions. Comparison of heme reduction potentials and amino acid sequences in the heme environment of the cytochromes *c'* suggests that residue 71 in RSCP and its equivalents may be important in modulating the reduction potential. In those cytochromes *c'* where this residue is D or E (RCCP, CVCP, RRCP), the reduction potential is less positive. Interestingly, this residue is located in a mobile region in close proximity to the heme.⁵¹ The residues and conformation of this region may modulate heme redox potential by controlling heme propionate solvent accessibility, as has been previously suggested for cytochromes.⁵² Sequences with G at position 87 and its equivalents (RSCP, RCCP) have intermediate potential, those with A or S (RRCP, CVCP) have less positive potential, and those with Q in this position (ADCP, AXCP) have more positive reduction potential. These differences may be attributed to hydrophobic packing, because G and Q exhibit greater contact surface interaction with the heme. In RPCP, whose reduction potential is also more positive, a deletion in the amino acid sequence actually places F spatially in this position, again with an increased contact surface area.

Conclusions

The structure of cytochrome *c'* from *Rhodobacter sphaeroides* provides new insights into the structural features of this class of proteins that dictate dimer topology and mediate heme redox activity. Dimer topology is dictated by the size, shape, and disposition of the hydrophobic patch at the dimer interface, as well as the planarity and complementarity of the contact region. Heme iron reduction potential is controlled by the hydrophathy profile and hydrophobic packing of residues in the heme pocket, although solvent accessibility to the heme propionate may provide finer modulation. Cytochromes *c'* can be clearly classified into two groups, based on the presence of a bulky aromatic residue blocking the sixth distal heme ligand binding site, and the presence of a

solvent accessible channel between helices B and C. However, analysis of factors that influence the quaternary structure of RSCP has revealed more subtle distinction in dimer topology among the cytochromes *c'* and has provided new insights for the design of synthetic multimeric proteins that incorporate hemes.

Acknowledgments

We thank the W.M. Keck Foundation and the California State University Program for Education and Research in Biotechnology (CSUPERB) for support of the Center for Molecular Structure. LMR was supported by a grant from the National Institutes of Health Minority Scientist Development Program (R25 GM56820). HLA and SRH were supported by California State University Fullerton. We thank Drs George Feher and Ed Abresch for access to bacterial growth facilities at UCSD; Drs Christopher Meyer and Brian Schick for helpful discussion, and Brad Van Mourik for computer support; Rebecca Baumbach, Cari Eldred, Mai Hua, Mei Liu, and Dorothy Rodriguez for their contributions to this project. LLNL is operated by the University of California for the US DOE under contract W-7405-ENG-48.

References

- Ambler, R.P.; Bartsch, R.G.; Daniel, M.; Kamen, M.D.; McLellan, L.; Meyer, T.E.; Van Beeumen, J. *Proc. Natl. Acad. Sci. U.S.A.* **1981**, *78*, 6854–6857.
- Bartsch, R.G. In *The Photosynthetic Bacteria*; Clayton, R.K.; Sistrom, W.R., Eds.; Plenum: New York, 1978; pp. 249–280.
- Moore, G.R.; Pettigrew, G.W. *Cytochromes c: Evolutionary, Structural and Physicochemical Aspects*; Springer: New York, 1990; pp. 230–240.
- Cross, R.; Lloyd, D.; Poole, R.K.; Moir, J.W.B. *J. Bacteriol.* **2001**, *183*, 3050–3054.
- Cross, R.; Aish, J.; Paston, S.J.; Poole, R.K.; Moir, J.W.B. *J. Bacteriol.* **2000**, *182*, 1442–1447.
- Meyer, T.E.; Kamen, M.D. *Adv. Protein Chem.* **1982**, *35*, 105–212.
- Cusanovich, M.A. *Biochim. Biophys. Acta* **1971**, *236*, 238–241.
- Presnell, S.R.; Cohen, F.E. *Proc. Natl. Acad. Sci. U.S.A.* **1989**, *86*, 6592–6596.
- Shibata, N.; Iba, S.; Misaki, S.; Meyer, T.E.; Bartsch, R.G.; Cusanovich, M.A.; Morimoto, Y.; Higuchi, Y.; Yasuoka, N. *J. Mol. Biol.* **1998**, *284*, 751–760.
- Maltempo, M.M.; Moss, T.H. *Q. Rev. Biophys.* **1976**, *9*, 181–215.
- Weber, P.C.; Howard, A.; Huu Xuong, N.; Salemme, F.R. *J. Mol. Biol.* **1981**, *153*, 399–424.
- Ren, Z.; Meyer, T.; McRee, D.E. *J. Mol. Biol.* **1993**, *234*, 433–445.
- Finzel, B.C.; Weber, P.C.; Hardman, K.D.; Salemme, F.R. *J. Mol. Biol.* **1985**, *186*, 627–643.
- Yasui, M.; Harada, S.; Kai, Y.; Kasai, N.; Kusunoki, M.; Matstuura, Y. *J. Biochem. (Tokyo)* **1992**, *111*, 317–324.
- Dobbs, A.J.; Anderson, B.F.; Faber, H.R.; Baker, E.N. *Acta Crystallogr., Sect. D* **1996**, *52*, 356–368.
- Archer, M.; Banci, L.; Dikava, E.; Romao, M.J. *J. Biol. Inorg. Chem.* **1997**, *2*, 611–622.
- Kassner, R.J. *Biochim. Biophys. Acta* **1991**, *1058*, 8–12.
- Lawson, D.M.; Stevenson, C.E.; Andrew, C.R.; Eady, R.R. *EMBO J.* **2000**, *19*, 5661–5671.
- Tahirov, T.; Masaki, S.; Meyer, T.E.; Cusanovich, M.A.; Higuchi, Y.; Yasuoka, N. *J. Mol. Biol.* **1996**, *259*, 467–479.
- Ramirez, L. Masters Thesis, California State University, Fullerton, CA, 2002.
- Engh, R.A.; Huber, R. *Acta Crystallogr., Sect. A* **1991**, *47*, 392–400.
- Cruickshank, D.W.J. *Acta Crystallogr., Sect. D* **1999**, *55*, 583–601.
- Collaborative Computational Project, Number 4. The CCP4 suite: Programs for protein crystallography. *Acta Crystallogr., Sect. D* **1994**, *50*, 760–763.
- Murshudov, G.N.; Vagin, A.A.; Dodson, E.J. *Acta Crystallogr., Sect. D* **1997**, *53*, 240–255.
- Otwinowski, Z.; Minor, W. *Methods Enzymol.* **1997**, *276*, 307–326.
- Kissinger, C.A.; Gehlhaar, D.K. *Acta Crystallogr., Sect. D* **1999**, *55*, 484–491.
- Rupp, B.; Segelke, B.W.; Zemla, A. American Crystallographic Association Meeting, San Antonio, TX, 2002; Series 2, Vol. 29.
- Lamzin, V.S.; Wilson, K.S. *Acta Crystallogr., Sect. D* **1993**, *49*, 129–147.
- Perrakis, A.; Sixma, T.K.; Wilson, K.S.; Lamzin, V.S. *Acta Crystallogr., Sect. D* **1997**, *53*, 448–455.
- McRee, D.E. *J. Mol. Graph.* **1992**, *10*, 44–46.
- Laskowski, R.A.; MacArthur, M.W.; Moss, D.S.; Thornton, J.M. *J. Appl. Crystallogr.* **1993**, *26*, 283–291.
- Choudhary, M.; Mackenzie, C.; Mouncey, N.J.; Kaplan, S. *Nucleic Acids Res.* **1999**, *27*, 61–62.
- Suwata, A.; Kaplan, S. *J. Bacteriol.* **1989**, *171*, 5850–5859.
- Nereng, K.S.; Kaplan, S. *J. Bacteriol.* **1999**, *181*, 1684–1688.
- Hutchinson, E.G.; Thornton, J.M. *Protein Sci.* **1996**, *5*, 212–220.
- Doyle, M.L.; Gill, S.J.; Cusanovich, M.A. *Biochemistry* **1986**, *23*, 2509–2516.
- Sobolev, V.; Sorokine, A.; Prilusky, J.; Abola, E.E.; Edelman, M. *Bioinformatics* **1999**, *15*, 327–332.
- Jones, S.; Thornton, J.M. *Proc. Natl. Acad. Sci. U.S.A.* **1996**, *93*, 13–20.
- Tahirov, T.H.; Misaki, S.; Meyer, T.E.; Cusanovich, M.A.; Higuchi, Y.; Yasuoka, N. *Nat. Struct. Biol.* **1996**, *3*, 459–464.
- Wallace, A.C.; Laskowski, R.A.; Thornton, J.M. *Protein Eng.* **1995**, *8*, 127–134.
- Kassner, R.J. *Proc. Natl. Acad. Sci. U.S.A.* **1972**, *69*, 2263–2267.
- Kassner, R.J.L. *J. Am. Chem. Soc.* **1973**, *95*, 2674–2677.
- Gibney, B.R.; Dutton, P.L. *Adv. Inorg. Chem.* **2001**, *52*, 409–454.
- Springs, S.L.; Bass, S.E.; McLendon, G.L. *Biochemistry* **2000**, *39*, 6075–6082.
- Fahnenschmidt, M.; Bittl, R.; Rau, H.K.; Haehnel, W.; Lubitz, W. *Chem. Phys. Lett.* **2000**, *323*, 329–339.
- Huffman, D.L.; Suslick, K.S. *Inorg. Chem.* **2000**, *39*, 5418–5419.

47. Shifman, J.M.; Gibney, B.R.; Sharp, R.E.; Dutton, P.L. *Biochemistry* **2000**, *39*, 14813–14821.
48. Gibney, B.R.; Huang, S.S.; Skalicky, J.J.; Fuentes, E.J.; Wand, A.J.; Dutton, P.L. *Biochemistry* **2001**, *40*, 10550–10561.
49. Kyte, J.; Doolittle, R.F. *J. Mol. Biol.* **1982**, *157*, 105–142.
50. Hopp, T.P.; Woods, K.R. *Proc. Natl. Acad. Sci. U.S.A.* **1981**, *78*, 3824–3828.
51. Caffrey, M.; Simorre, J.-P.; Brutscher, B.; Cusanovich, M.; Marion, D. *Biochemistry* **1995**, *34*, 5904–5912.
52. Bertrand, P.; Mbarki, O.; Asso, M.; Blanchard, L.; Guerlesquin, F.; Tegoni, M. *Biochemistry* **1995**, *34*, 11071–11079.